High-Spin and Low-Spin α-Picolylamine Iron(II) Complexes. Effect of Ligand Reversal on Spin State

Anthony M. Greenaway and Ekk Sinn*

Contribution from the Department of Chemistry, University of Virginia, Charlottesville, Virginia 22901. *Received May 16, 1978*

Abstract: The magnetic properties and single crystal structures of the α-picolylamine (α-P) complexes, $[Fe(\alpha\text{-}P)_3]Cl_2\cdot 2H_2O$ and $[Fe(\alpha\text{-}P)_3]Cl_2\cdot CH_3OH$, have been studied in order to discover the relationship between spin state and molecular structure. The dihydrate solvate is low spin at room temperature and below, while the methanol solvate is high spin at room temperature, undergoing a transition to low spin in the region 100–200 K. The room temperature molecular structures of the two complexes exhibit some major differences. The hydrate complex has all three ligands related approximately chirally so that the $[Fe(\alpha\text{-}P)_3]^{2+}$ ion has approximate threefold symmetry. However, the methanol solvate has one of the ligands coordinated with both of its donor atoms reversed. This difference is attributed to hydrogen bonding which occurs only in the dihydrate. The pseudo-threefold axis places all three amine nitrogen atoms on one side of the ion, thereby facilitating hydrogen bonding between the amine nitrogens and the water molecules. This hydrogen bonding is absent in the methanol solvate, and the structure that it exhibits is presumably the more stable one in the absence of hydrogen bonding. The average metal-ligand bond distance, ⟨Fe–N⟩, is 0.192 Å larger in the high-spin methanol solvate than in the low-spin complex. This is the largest value ever observed for the bond length difference between high-spin and low-spin states. Crystal data for $[Fe(\alpha\text{-}P)_3]Cl_2\cdot 2H_2O$ follow: space group $P\bar{1}$, $Z = 2$, $a = 10.142$ (2) Å, $b = 10.651$ (4) Å, $c = 11.351$ (2) Å, $\alpha = 113.89$ (2)°, $\beta = 98.50$ (2)°, $\gamma = 93.97$ (2)°, $V = 1097$ Å^3, $R = 3.3\%$ for 3180 reflections. Crystal data for $[Fe(\alpha\text{-}P)_3]Cl_2\cdot CH_3OH$ follow: space group $Pbca$, $Z = 8$, $a = 22.428$ (6) Å, $b = 11.524$ (2) Å, $c = 18.906$ (5) Å, $V = 4887$ Å^3, $R = 4.1\%$ for 1712 reflections.

Introduction

Transition metal complexes lying near the high-spin ⇆ low-spin crossover have been shown to be very sensitive to changes in temperature and pressure, minor chemical changes in the ligands, counteranions in the case of cationic complexes, and solvent molecules occluded in the lattice.[1-11] The effect on spin state equilibria of solvent molecules in the solid state lattice is quite dramatic. In the neutral ferric dithiocarbamate molecules, benzene or nitrobenzene molecules in the lattice shift the equilibrium toward low spin to the same extent as temperature decreases of hundreds of degrees or pressure increases of thousands of atmospheres. On the other hand, inclusion of hydrogen bonding solvents such as chloroform, dichloromethane, or water tends to shift the equilibrium toward the high-spin side in addition to apparently drastically lowering the energy of the intermediate $S = 3/2$ spin state.[5-8] In the complexes $[Fe(sal)trien]^+X^-$ (where X = Cl, NO_3) inclusion of water molecules, simultaneously hydrogen bonded to both the cation and the anion, induces a low spin state, while analogous anhydrous complexes tend to be pure high spin or to exhibit the high-spin–low-spin equilibrium.[9] The mode of action of non-hydrogen-bonding solvents such as benzene and nitrobenzene in promoting low-spin states is unclear, but the solvents capable of hydrogen bonding clearly all act via hydrogen-bonding interactions with ligand donor atoms of the complexes.

The complexes $[Fe(\alpha\text{-}P)_3]Cl_2\cdot xS$ (where α-P = α-picolylamine and xS = CH_3OH, C_2H_5OH, or $2H_2O$) are of interest because their Mössbauer spectra provide strong evidence of different spin states and of spin-state crossovers in some cases. These compounds were therefore considered to be capable of providing good evidence for the way in which hydrogen-bonding interactions influence the transition metal spin state: in this case each of the solvents is capable of hydrogen-bonding interaction, though to a differing extent.

A further interest in comparing the structures of the two $[Fe(\alpha\text{-}P)_3]^{2+}$ complexes centers around the structural differences in the immediate vicinity of the central metal atom, especially in the metal–ligand bond lengths (r). A bond-length difference (δ) between high- (r_h) and low-spin (r_l) states of about 0.12–0.13 Å has been observed in a wide range of iron(III) complexes, in which the spin-state change involves the transfer of two electrons from the t_{2g} to the e_g orbitals. In iron(II) complexes, the spin-state change involves the same electron transfer, and a similar average metal–ligand bond-length change might well be expected, although at present no accurate data are available for iron(II). Low-accuracy data have been obtained for $[Fe(phen)_2(NCS)_2]$[15] at 295 K (R = 21%) and around 100 K (19%) leading to a metal–ligand bond-length difference, δ, of 0.12 Å. Data with high R values should in any case be treated with caution: similar low-accuracy data on tris(pyrrolidyldithiocarbamate)iron(III)[16] has lead to a gross underestimate of δ. The present pair of compounds provides some surprises in this regard.

Experimental Section

The complexes were prepared as described[13,14] by Sorai et al. The syntheses were carried out using Schlenk apparatus, and the recrystallizations and all product handling were carried out in a dry nitrogen atmosphere. Magnetic susceptibilities and moments were determined using a superconducting susceptometer incorporating a Josephson junction magnetometer, superconducting magnets, and shields.[7]

Crystal data for $[Fe(\alpha\text{-}P)_3]Cl_2\cdot 2H_2O$: $FeCl_2O_2N_6C_{18}H_{28}$, mol wt 487, space group $P\bar{1}$, $Z = 2$, $a = 10.142$ (2) Å, $b = 10.651$ (4) Å, $c = 11.351$ (2) Å, $\alpha = 113.89$ (2)°, $\beta = 98.50$ (2)°, $\gamma = 93.97$ (2)°, $V = 1097$ Å^3, $\rho_{calcd} = 1.47$ g cm^{-3}, $\rho_{obsd} = 1.49$ g cm^{-3}, μ(Mo Kα) = 9.8 cm^{-1}; the crystal used was a fragment which was very approximately rounded to fit it into a capillary.

Crystal data for $[Fe(\alpha\text{-}P)_3]Cl_2\cdot CH_3OH$: $FeCl_2ON_6C_{19}H_{28}$, mol wt 482, space group $Pbca$, $Z = 8$, $a = 22.428$ (6) Å, $b = 11.524$ (2) Å, $c = 18.906$ (5) Å, $V = 4887$ Å^3, $\rho_{calcd} = 1.314$ g cm^{-3}, $\rho_{obsd} = 1.308$ g cm^{-3}, μ(Mo Kα) = 8.7 cm^{-1}; crystal dimensions (in mm from centroid) (210) 0.20, ($\bar{2}10$) 0.20, ($2\bar{1}0$) 0.20, ($\bar{2}\bar{1}0$) 0.20, (001) 0.035, (00$\bar{1}$) 0.035; max, min transmission coefficients, 0.96, 0.92.

The single crystals for X-ray diffraction studies were mounted in glass capillaries in a nitrogen atmosphere to protect them from oxygen and water.

For each crystal, the Enraf-Nonius program SEARCH was used to obtain 25 accurately centered reflections which were then used in the program INDEX to obtain approximate cell dimensions and an orientation matrix for data collection. Refined cell dimensions and their estimated standard deviations were obtained from least-squares refinement of 25 accurately centered reflections. The mosaicity of the crystals was examined by the ω-scan technique and judged to be satisfactory.

0002-7863/78/1500-8080$01.00/0

Table II

Bond Lengths (Å) for the Complexes $[Fe(\alpha\text{-}P)_3]Cl_2 \cdot xS$, Where $xS = 2H_2O$ and CH_3OH

	$2H_2O$	CH_3OH		$2H_2O$	CH_3OH
Fe-N(11)	1.979 (1)	2.188 (4)	N(31)-C(32)	1.347 (2)	1.352 (6)
Fe-N(18)	2.030 (1)	2.178 (4)	N(31)-C(36)	1.353 (2)	1.344 (6)
Fe-N(21)	1.987 (1)	2.218 (4)	N(38)-C(37)	1.475 (2)	1.469 (6)
Fe-N(28)	2.021 (1)	2.192 (4)	C(12)-C(13)	1.385 (2)	1.380 (8)
Fe-N(31)	1.991 (1)	2.223 (4)	C(12)-C(17)	1.490 (2)	1.487 (8)
Fe-N(38)	2.026 (1)	2.189 (4)	C(13)-C(14)	1.373 (2)	1.372 (8)
N(11)-C(12)	1.356 (2)	1.324 (6)	C(14)-C(15)	1.379 (2)	1.370 (8)
N(11)-C(16)	1.360 (2)	1.327 (6)	C(15)-C(16)	1.365 (2)	1.370 (8)
N(18)-C(17)	1.478 (2)	1.479 (7)	C(22)-C(23)	1.391 (2)	1.377 (7)
N(21)-C(22)	1.343 (2)	1.335 (6)	C(22)-C(27)	1.505 (2)	1.504 (7)
N(21)-C(26)	1.351 (2)	1.352 (7)	C(23)-C(24)	1.377 (2)	1.364 (8)
N(28)-C(27)	1.466 (2)	1.487 (6)	C(24)-C(25)	1.372 (2)	1.389 (8)
			C(25)-C(26)	1.377 (2)	1.361 (7)
			C(32)-C(33)	1.378 (2)	1.379 (7)
			C(32)-C(37)	1.504 (2)	1.489 (7)
			C(33)-C(34)	1.380 (2)	1.379 (7)
			C(34)-C(35)	1.383 (2)	1.367 (7)
			C(35)-C(36)	1.362 (2)	1.371 (7)

Hydrogen Bonding Interactions for $[Fe(\alpha\text{-}P)_3]Cl_2 \cdot 2H_2O$

molecule 1	molecule 2	distance, Å
Cl(1)	N(38)[a]	3.262
	O(1)[b]	3.308
	N(38)[c]	3.353
Cl(2)	O(2)[d]	3.187
	O(1)[c]	3.228
	N(28)[b]	3.303
	O(2)[c]	3.393
O(1)	N(18)[b]	3.102
	N(18)[c]	3.494

[a] $x, 1 + y, z$. [b] x, y, z. [c] $1 - x, 1 - y, 1 - z$. [d] $x, y, 1 + z$.

Collection and Reduction of Data. Diffraction data were collected at 292 K on an Enraf-Nonius four-circle CAD-4 diffractometer controlled by a PDP8/M computer, using Mo Kα radiation from a highly oriented graphite crystal monochromator. The θ-2θ scan technique was used to record the intensities for all nonequivalent reflections for which $1° < 2\theta < 47°$ for $[Fe(\alpha\text{-}P)_3]Cl_2 \cdot 2H_2O$ and $1° < 2\theta < 45°$ for $[Fe(\alpha\text{-}P)_3]Cl_2 \cdot CH_3OH$. Scan widths (SW) were calculated from the formula $SW = A + B \tan\theta$ where A is estimated from the mosaicity of the crystal and B allows for the increase in peak width due to $K\alpha_1$-$K\alpha_2$ splitting. The values of A and B were 0.6 and 0.35°, respectively, for both complexes. The calculated scan angle is extended at each side by 25% for background determination (BG1 and BG2). The net count is then calculated as NC = TOT − 2(BG1 + BG2) where TOT is the integrated peak intensity. Reflection data were considered insignificant if intensities registered less than 10 counts above background on a rapid prescan, such reflections being rejected automatically by the computer.

The intensities of four standard reflections, monitored at 100 reflection intervals, showed no greater fluctuations during the data collection than those expected from Poisson statistics. The raw intensity data were corrected for Lorentz-polarization effects (including the polarization effect of the crystal monochromator) and then for absorption. Spherical absorption corrections were applied to the $[Fe(\alpha\text{-}P)_3]Cl_2 \cdot 2H_2O$ data. After the intensities of equivalent reflections were averaged, the data were reduced to 3412 independent intensities for $[Fe(\alpha\text{-}P)_3]Cl_2 \cdot 2H_2O$ and 2966 for $[Fe(\alpha\text{-}P)_3]Cl_2 \cdot CH_3OH$ of which 3180 for $[Fe(\alpha\text{-}P)_3]Cl_2 \cdot 2H_2O$ and 1712 for $[Fe(\alpha\text{-}P)_3]Cl_2 \cdot CH_3OH$ had $F_o^2 > 3\sigma(F_o^2)$, where $\sigma(F_o^2)$ was estimated from counting statistics.[17] These data were used in the final refinement of the structural parameters.

Determination and Refinement of the Structures. The positions of the metal and all the ligand atoms in the dihydrate complex and those of the metal, one chlorine, and one of the ligand nitrogen atoms in the methanol solvate were determined from three-dimensional Patterson functions calculated from all the intensity data. For each crystal the intensity data were phased sufficiently well by these positional coordinates to permit location of the remaining nonhydrogen and some of the hydrogen atoms.

Full-matrix least-squares refinement was based on F, and the function minimized was $\Sigma w(|F_o| - |F_c|)^2$. The weights w were then taken as $[2F_o/\sigma(F_o^2)]^2$, where $|F_o|$ and $|F_c|$ are the observed and calculated structure factor amplitudes. The atomic scattering factors for nonhydrogen atoms were taken from Cromer and Waber[18] and those for hydrogen from Stewart et al.[19] The effects of anomalous dispersion for all nonhydrogen atoms were included in F_c using the values of Cromer and Ibers[20] for $\Delta f'$ and $\Delta f''$. Agreement factors are defined as $R = \Sigma||F_o| - |F_c||/\Sigma|F_o|$ and $R_w = (\Sigma w(|F_o| - |F_c|)^2/\Sigma w|F_o|^2)^{1/2}$. To minimize computer time, the initial calculations were carried out on the first 1000 reflections collected.

Anisotropic temperature factors were introduced for all nonhydrogen atoms. Further Fourier difference functions permitted location of the remaining hydrogen atoms except for those on the methanol molecule in $[Fe(\alpha\text{-}P)_3]Cl_2 \cdot CH_3OH$. The hydrogen atoms were included in the refinement with fixed temperature factors (5.0 Å^2). The models converged with $R = 3.3$, $R_w = 4.6\%$ for $[Fe(\alpha\text{-}P)_3]Cl_2 \cdot 2H_2O$ and $R = 4.1$, $R_w = 5.0\%$ for $[Fe(\alpha\text{-}P)_3]Cl_2 \cdot CH_3OH$. A structure factor calculation with all observed and unobserved reflections included (no refinement) gave $R = 3.9$, 5.9% for the two compounds, respectively; on this basis it was decided that careful measurement of reflections rejected automatically during data collection would not significantly improve the results. A final Fourier difference function was featureless. Tables of the observed structure factors are available.[21] The principal programs used are as previously described.[22]

Results and Discussion

Final positional and thermal parameters for $[Fe(\alpha\text{-}P)_3]Cl_2 \cdot 2H_2O$ and $[Fe(\alpha\text{-}P)_3]Cl_2 \cdot CH_3OH$ are given in Table I.[21] Tables II and III contain the bond lengths and angles. The digits in parentheses in the tables are the estimated standard deviations in the least significant figures quoted, and were derived from the inverse matrix in the course of least-squares

Table III. Bond Angles (deg) for the Complexes $[Fe(\alpha\text{-}P)_3]Cl_2 \cdot xS$ Where $xS = 2H_2O$ and CH_3OH

	$2H_2O$	CH_3OH		$2H_2O$	CH_3OH
N(11)-Fe-N(18)	82.29 (4)	76.9 (2)	Fe-N(31)-C(32)	115.52 (8)	115.5 (3)
N(11)-Fe-N(21)	94.73 (4)	160.4 (2)	Fe-N(31)-C(36)	127.44 (9)	126.6 (4)
N(11)-Fe-N(28)	173.99 (4)	89.9 (2)	C(32)-N(31)-C(36)	117.0 (1)	117.6 (5)
N(11)-Fe-N(31)	96.15 (4)	96.9 (2)	Fe-N(38)-C(37)	108.19 (8)	112.1 (3)
N(11)-Fe-N(38)	90.28 (4)	98.8 (2)	N(11)-C(12)-C(13)	121.7 (1)	121.6 (6)
N(18)-Fe-N(21)	89.78 (5)	93.4 (2)	N(11)-C(12)-C(17)	115.1 (1)	117.4 (5)
N(18)-Fe-N(28)	92.10 (5)	101.7 (2)	C(13)-C(12)-C(17)	123.1 (1)	121.0 (6)
N(18)-Fe-N(31)	174.71 (4)	162.1 (2)	C(12)-C(13)-C(14)	119.5 (1)	119.9 (6)
N(18)-Fe-N(38)	94.19 (5)	88.7 (2)	C(13)-C(14)-C(15)	119.3 (1)	118.3 (6)
N(21)-Fe-N(28)	83.08 (4)	75.2 (2)	C(14)-C(15)-C(16)	118.7 (1)	118.4 (6)
N(21)-Fe-N(31)	95.39 (4)	97.1 (2)	N(11)-C(16)-C(15)	123.3 (1)	123.7 (5)
N(21)-Fe-N(38)	174.00 (4)	98.0 (2)	N(18)-C(17)-C(12)	109.9 (1)	112.0 (5)
N(28)-Fe-N(31)	89.63 (4)	95.0 (2)	N(21)-C(22)-C(23)	121.8 (1)	122.4 (6)
N(28)-Fe-N(38)	92.27 (4)	167.8 (2)	N(21)-C(22)-C(27)	116.4 (1)	116.6 (5)
N(31)-Fe-N(38)	80.75 (4)	75.6 (2)	C(23)-C(22)-C(27)	121.8 (1)	120.9 (5)
Fe-N(11)-C(12)	115.56 (9)	115.4 (4)	C(22)-C(23)-C(24)	119.9 (1)	119.1 (6)
Fe-N(11)-C(16)	127.16 (9)	126.3 (4)	C(23)-C(24)-C(25)	118.5 (1)	119.9 (6)
C(12)-N(11)-C(16)	117.2 (1)	118.1 (5)	C(24)-C(25)-C(26)	119.1 (1)	117.3 (6)
Fe-N(18)-C(17)	109.68 (8)	110.2 (3)	N(21)-C(26)-C(25)	123.2 (1)	124.0 (5)
Fe-N(21)-C(22)	115.74 (9)	116.0 (4)	N(28)-C(27)-C(22)	111.9 (1)	111.0 (4)
Fe-N(21)-C(26)	126.82 (9)	126.8 (4)	N(31)-C(32)-C(33)	122.3 (1)	121.7 (5)
C(22)-N(21)-C(26)	117.4 (1)	117.3 (5)	N(31)-C(32)-C(37)	114.2 (1)	116.8 (5)
Fe-N(28)-C(27)	112.08 (8)	110.5 (3)	C(33)-C(32)-C(37)	123.5 (1)	121.5 (5)
C(32)-C(33)-C(34)	119.6 (1)	119.1 (5)			
C(33)-C(34)-C(35)	118.5 (1)	119.8 (5)			
C(34)-C(35)-C(36)	118.9 (1)	118.2 (5)			
N(31)-C(36)-C(35)	123.7 (1)	123.5 (5)			
N(38)-C(37)-C(32)	108.6 (1)	111.5 (5)			

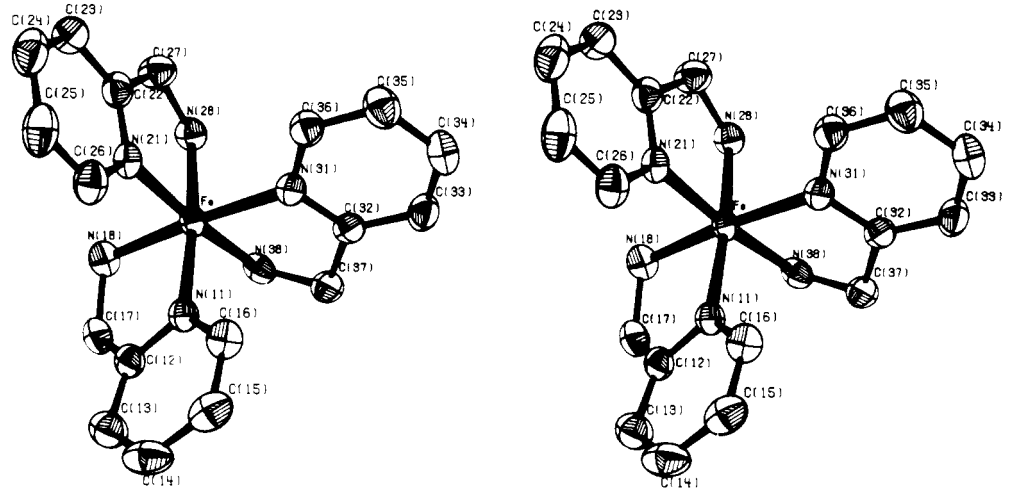

Figure 1. Stereoscopic pair view of $[Fe(\alpha\text{-}P)_3]^{2+}$ in $[Fe(\alpha\text{-}P)_3]Cl_2 \cdot 2H_2O$.

refinement calculations. Figures 1 and 2 are stereoscopic pair views of the two molecules, respectively, while Figures 3 and 4 show the molecular packing in the unit cells of the same compounds.

The most significant difference between the two compounds other than their spin states is the presence of a pseudo-threefold axis for the entire $[Fe(\alpha\text{-}P)_3]^{2+}$ in the dihydrate solvate, and its absence in the methanol analogue. In the dihydrate, a 120° rotation will approximately transform ligand 1 into ligand 2, and then into ligand 3 via a further 120° rotation. However, in the methanol solvate, the same would only be true if ligand 2 were detached and turned over (180°) such as to interchange N(1) and N(8). Both complexes still have pseudo-threefold symmetry for just the FeN_6 chromophore, however. This is illustrated schematically in Figure 5. The extent of trigonal distortion in each complex is indicated by the magnitude of the average twist angle, ϕ, which is 53.7° for the $2H_2O$ complex and 41.1° for the CH_3OH complex (a regular octahedron requires 60° and a trigonal bipyramid 0°).

Although the reversal of one of the ligands in the methanol solvate must contribute to the difference in the average twist angle ϕ, the spin state difference between the two complexes is likely to be the most important factor. The difference in ϕ between the two spin states is as expected from the large metal–ligand bond length change: if the distance between the pyridine and the amino nitrogen atoms of each ligand is assumed to be fixed, then a drastic increase in the metal–ligand bond length is most easily accommodated by a twist about the pseudo-C_3 axis such as to reduce ϕ (Figure 5). The other deviations from regular octahedral geometry appear to derive mainly from the trigonal distortion (indicated by the extent that ϕ falls below 60°) and from the asymmetrical nature of ligand coordination in the methanol solvent. Both these effects work to make the FeN_6 chromophore more distorted in

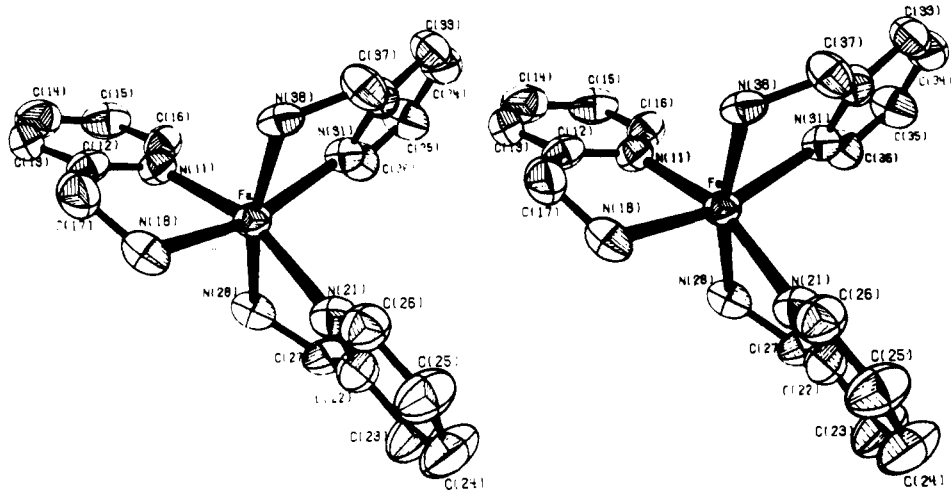

Figure 2. Stereoscopic pair view of $[Fe(\alpha\text{-}P)_3]^{2+}$ in $[Fe(\alpha\text{-}P)_3]Cl_2\cdot CH_3OH$.

$[Fe(\alpha\text{-}P)_3]Cl_2\cdot CH_3OH$ than in $[Fe(\alpha\text{-}P)_3]Cl_2\cdot 2H_2O$, as is clearly indicated by the N-Fe-N bond angles in Table III.

Hydrogen-bonding interactions between the $[Fe(\alpha\text{-}P)_3]^{2+}$ cations and the water molecules and in turn between the water and the Cl^- anions occur in $[Fe(\alpha\text{-}P)_3]Cl_2\cdot 2H_2O$, to produce an infinite polymeric network. However, no corresponding hydrogen bonding interactions occur in the methanol solvate, which has only a $CH_3OH\cdots Cl^-$ interaction. The hydrogen bonding in the dihydrate complex is clearly facilitated by the pseudo-threefold axis which places all the amino groups on the same triangular face of the octahedral cation. Since there are no other evident mechanisms, we propose that the hydrogen bonding is the driving force that leads to the threefold geometry of Figure 5a. The configuration of Figure 5b, adopted by the methanol solvate, is presumably slightly more stable in the absence of hydrogen bonding.

Hydrogen bonding of water molecules to both cationic complexes and counteranions is associated with low-spin states in iron(III) complexes which would otherwise have been high spin, or at the spin-state crossover.[9] This behavior is also observed for the $[Fe(\alpha\text{-}P)_3]^{2+}$ system. This common feature permits the generalization that such hydrogen-bonding interactions favor spin pairing and that therefore spin crossover complexes which are salts are more likely to be low spin if they crystallize as hydrates.

The magnetic properties of the $[Fe(\alpha\text{-}P)_3]Cl_2\cdot CH_3OH$ complex are shown in Figure 6. The diaquo solvate is low spin (t_{2g}^6) over the temperature range, as expected from the Mössbauer data,[13,14] with a magnetic moment of about 0.6 μ_B, while the methanol solvate is only low spin below 90 K: between 100 and 200 K the magnetic moment rises sharply, and continues to rise slightly above 200 K to the value expected for high-spin ($t_{2g}^4e_g^2$) iron(II). The complex is 90, 50, and 10% high spin at 191, 153, and 115 K, respectively. No hysteresis was found on cooling and warming. Renovitch et al.[12] have reported the magnetic behavior of $[Fe(\alpha\text{-}P)_3]X_2$ (X = Cl, Br, I) but make no mention of possible solvate molecules. These results correspond closely to those obtained from Mössbauer.[13,14] Thus we can correlate the structures, Mössbauer spectra, and magnetic properties of the complexes. It is clear that at room temperature, the diaquo and methanol solvates may be considered as low-spin and high-spin FeN_6 compounds, respectively. From the reported Mössbauer spectra,[13,14] it now appears that the previously reported magnetic data[12] correspond to the ethanol solvate. Further studies are being carried out to confirm this.

The difference between average metal-ligand bond lengths in the high-spin and low-spin complexes, δ, is no less than 0.192

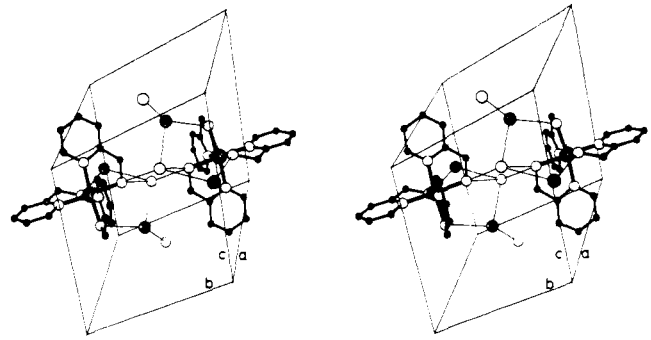

Figure 3. Molecular packing in the unit cell of $[Fe(\alpha\text{-}P)_3]Cl_2\cdot 2H_2O$.

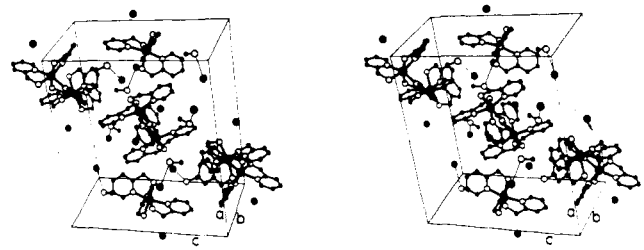

Figure 4. Molecular packing in the unit cell of $[Fe(\alpha\text{-}P)_3]Cl_2\cdot CH_3OH$.

Å, which is surprising to say the least, in view of earlier measurements. However, these are by far the most accurate data for spin-state crossover systems in iron(II); indeed they are the only truely accurate data so far available. Moreover, we believe that such a large value of δ can readily be rationalized. Detailed comparisons have been made for various md^n configurations in analogous complexes and essentially the same ligand environment for the metals involved.[23] These results showed that pairing of electrons, especially in the t_{2g} subshell, cause a significant reduction in the metal–ligand bond length. This was especially true of low-spin d^6 where all the electrons are paired. Thus the d^6 cobalt(III) dithiocarbamates had a markedly shorter average metal–ligand bond (2.275 Å) than other complexes which have only unpaired t_{2g} electrons, viz. d^3 (2.406 Å in Cr(III)). For low-spin $3d^5$ (t_{2g}^5), the average metal–ligand bond is about 2.31 Å (in Fe(III) complexes),[7,9] which is still longer than in t_{2g}^6. Addition of an e_g electron increases the bond length markedly (2.461 Å in Mn(III) $t_{2g}^3e_g^1$ compared with 2.406 Å in Cr(III) t_{2g}^3);[22] the addition of two e_g electron likewise produces an increase to 2.44 Å in high-spin Fe(III) $t_{2g}^3e_g^2$.[7,9] Thus if we assume that we can approximately

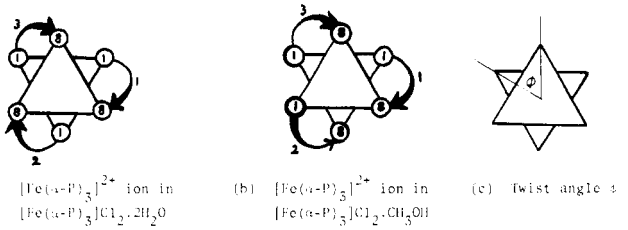

Figure 5. (a) Configuration of $[Fe(\alpha\text{-}P)_3]^{2+}$ ion in $[Fe(\alpha\text{-}P)_3]Cl_2 \cdot 2H_2O$. (b) Configuration of $[Fe(\alpha\text{-}P)_3]^{2+}$ ion in $[Fe(\alpha\text{-}P)_3]Cl_2 \cdot CH_3OH$. (c) Twist angle ϕ.

separate the contributions of t_{2g} and e_g subshells to δ, then the e_g contribution is approximately the same for analogous iron(II) and iron(III) systems. In each case the population difference being considered is between e_g^2 and e_g^0. On the other hand, the t_{2g} subset makes a significant contribution, and a negative one, only when a t_{2g}^6 configuration arises. This negative contribution to iron(II) is then additional to the amount normally observed in iron(III).

The large value for δ for these compounds suggests a large value for iron(II) spin-state equilibria in general, although more work is needed to establish what variation exists for iron(II) complexes. Our contention that δ is larger in general for iron(II) than for iron(III) spin-state crossovers is compatible with the fact that all known iron(II) spin-state equilibria have relatively slow interconversion rates (e.g., compared to Mössbauer relaxation time) unlike many of those for iron(III). The greater structural change required of spin-state interconversion in iron(II) would raise the activation energy for the process and thereby reduce the rate. Of course this is not the only mechanism affecting the interconversion rate; it seems likely that spin-orbit coupling mixing would increase the rate of spin interconversion. Thus the greater spin-orbit coupling constant of the ligand atoms would lead to the observed faster interconversion rate in the FeS_6 chromophore in the dithiocarbamates than in the FeS_3O_3 and FeO_2N_4 chromophore of other complexes. However, with a structural change as dramatic as the metal-ligand bond-length change observed here, structural factors are expected to be dominant.

The ligand reversal is expected to be permanent in the methanol solvate, at all temperatures, and the $[Fe(\alpha\text{-}P)]Cl_2 \cdot 2H_2O$ complex therefore does not give an accurate representation of the structure of the $[Fe(\alpha\text{-}P)]^{2+}$ ion in the low-temperature form of the $[Fe(\alpha\text{-}P)_3]Cl_2 \cdot CH_3OH$. However, there is no reason to expect any significant differences in the average metal-ligand bond lengths of the two low-spin forms. We may now also postulate the ligand-reversed structure of Figure 5b for the monohydrate complex which must have a reduced capacity for hydrogen bonding compared to the dihydrate, and which exhibits a spin-state crossover, like the methanol solvate.[13,14] In practice, the monohydrate, when obtained by heating, may contain a mixture of both configurations.

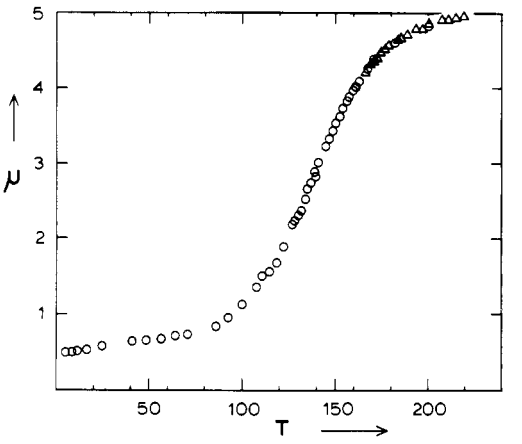

Figure 6. Observed magnetic moments μ (μ_B) for $[Fe(\alpha\text{-}P)_3]Cl_2 \cdot CH_3OH$ as a function of absolute temperature T (K): O, warming; Δ, cooling.

Supplementary Material Available: Positional and thermal parameters and observed and calculated structure factors (26 pages). Ordering information is given on any current masthead page.

References and Notes

(1) A. H. Ewald, R. L. Martin, E. Sinn, and A. H. White, *Inorg. Chem.*, **8**, 1837 (1969).
(2) C. M. Harris, T. N. Lockyer, R. L. Martin, H. R. H. Patil, E. Sinn, and I. M. Stewart, *Aust. J. Chem.*, **22**, 2105 (1969).
(3) R. N. Sylva and H. A. Goodwin, *Aust. J. Chem.*, **20**, 479 (1967).
(4) C. M. Harris and E. Sinn, *Inorg. Chim. Acta*, **2**, 296 (1967).
(5) R. J. Butcher and E. Sinn, *J. Am. Chem. Soc.*, **98**, 2440 (1976).
(6) R. J. Butcher and E. Sinn, *J. Am. Chem. Soc.*, **98**, 5159 (1976).
(7) E. J. Cukauskas, B. S. Deaver, Jr., and E. Sinn, *J. Chem. Phys.*, **67**, 1257 (1977).
(8) E. J. Cukauskas, B. S. Deaver, Jr., and E. Sinn, *Inorg. Nucl. Chem. Lett.*, **13**, 283 (1977).
(9) E. Sinn, P. G. Sim, E. V. Dose, M. F. Tweedle, and L. J. Wilson, *J. Am. Chem. Soc.*, in press.
(10) M. F. Tweedle and L. J. Wilson, *J. Am. Chem. Soc.*, **98**, 4824 (1976).
(11) S. Mitra, A. H. White, and C. L. Raston, *Aust. J. Chem.*, **29**, 1897 (1976).
(12) G. A. Renovitch and W. A. Baker, Jr., *J. Am. Chem. Soc.*, **89**, 6377 (1967).
(13) M. Sorai, J. Ensling, and P. Gütlich, *Chem. Phys.*, **18**, 199 (1976).
(14) M. Sorai, J. Ensling, K. M. Hasselbach, and P. Gütlich, *Chem. Phys.*, **20**, 197 (1977).
(15) E. König and K. J. Watson, *Chem. Phys. Lett.*, **6**, 457 (1970).
(16) P. C. Healy and A. H. White, *J. Chem. Soc., Dalton Trans.*, 1163 (1972).
(17) P. W. R. Corfield, R. J. Doedens, and J. A. Ibers, *Inorg. Chem.*, **6**, 197 (1967).
(18) D. T. Cromer and J. T. Waber, "International Tables for X-ray Crystallography", Vol. IV, Kynoch Press, Birmingham, England, 1974.
(19) R. F. Stewart, E. R. Davidson, and W. T. Simpson, *J. Chem. Phys.*, **42**, 3175 (1965).
(20) D. T. Cromer and J. A. Ibers, ref 17.
(21) See paragraph at end of paper regarding supplementary material.
(22) D. P. Freyberg, G. M. Mockler, and E. Sinn, *J. Chem. Soc., Dalton Trans.*, 447 (1976).
(23) R. J. Butcher and E. Sinn, *J. Chem. Soc., Dalton Trans.*, 2518 (1975).